Physica B 524 (2017) 154–162

Contents lists available at ScienceDirect

Physica B

journal homepage: www.elsevier.com/locate/physb

Equation of state of liquid bismuth and its melting curve from ultrasonic investigation at high pressure

Chang Su[a], Yonggang Liu[a,*], Zhigang Wang[b], Wei Song[a], Paul.D. Asimow[c], Hongfeng Tang[a], Hongsen Xie[a]

[a] Key Laboratory of High-temperature and High-pressure Study of the Earth's Interior, Institute of Geochemistry, Chinese Academy of Sciences, Guiyang 550081, China
[b] National Key Laboratory of Shock Wave and Detonation Physics, Institute of Fluid Physics, Chinese Academy of Engineering Physics, Mianyang 621900, China
[c] Division of Geological and Planetary Sciences, California Institute of Technology, Pasadena 91125, USA

ARTICLE INFO

Keywords:
Liquid bismuth
Sound velocity
Equation of state
Melting curve

ABSTRACT

To obtain the equation of state of liquid bismuth and its melting curve, ultrasonic velocity measurements were performed in a multi-anvil apparatus. Using a series of thermodynamic relationships, we extract the volume of liquid bismuth as functions of pressure and temperature up to 973 K and 4.3 GPa. We also introduce a calculation process to build the thermal equations of state of each phase of solid bismuth based on their phase transition boundaries. Combining the thermodynamic parameters of liquid and solid bismuth, we employ the Gibbs equation and the Clausius-Clapeyron equation and finally derive the melting curve up to 8 GPa, which shows excellent consistency with most previous theoretical and experimental results. These results not only demonstrate the accuracy of our experimental and theoretical methods, but also demonstrate the feasibility of the thermodynamic method for obtaining unknown melting curves.

1. Introduction

Accurate melting curves and high-temperature and high-pressure (HTHP) equations of state (EOS) of metals have proven to be quite significant in condensed matter physics and geological research [1–3]. In geophysics and planetary science, it is important to obtain the behavior especially of iron but also those elements that might alloy with iron under extreme conditions [4–6]. For instance, thermodynamic parameters of these metals are used not only to constrain the chemical composition of the Earth's core, but also to estimate phase boundaries and thereby infer the temperature and energy budget of the interior of the Earth [7–9].

Although not directly relevant to geological sciences, a commonly studied analogue metal for HTHP property research is Bismuth (Bi). Bismuth is a post-transition metal with a complex phase diagram in the low temperature and pressure range (including the five solid phases referred to as I, II, III, IV, and V), which makes it useful both as a pressure calibrate and as a model system for other metals whose phase diagrams are less amenable to detailed study [10,11]. Based on compression in a hydrostatic gas pressure apparatus, Bridgman originally defined the phase transition pressure for Bi up to ~ 3 GPa [12]. Incorporating the piston cylinder data of Kennedy and Newton [13], Klement [10] extended the phase diagram for the solid phase transitions of Bi to ~ 7 GPa using a double-stage compression device and differential thermal analysis. Synthesizing this phase diagram and later studies [14,15], Chen [16] provided a more complete version which has an accurate III-V boundary.

Following the development of experimental methods that can achieve more extreme conditions, researchers have begun to concentrate on the equation of state (EOS) and the melting curve of Bi over a wider range of temperature and pressure. For example, the elastic properties of bcc (body centered cubic) Bi (phase V) have been measured up to a maximum of 222 GPa [17] with multiple techniques [17–20]. In parallel, although the crystal structures along the Hugoniot have not been positively identified, shock compression data define the shock-induced melting temperature [21–23].

As a supplement to direct experimental determinations, theoretical calculation is another commonly-used method to determine or extrapolate equations of state and melting curves. In 1975, Johnson et al. introduced a method based on the criterion of equal Gibbs energy of coexisting phases along their phase boundaries [24]. This approach was used by Cox [25] and Bai et al. [26] to calculate the Bi melting

* Corresponding author.
E-mail address: liuyonggang@vip.gyig.ac.cn (Y. Liu).

http://dx.doi.org/10.1016/j.physb.2017.08.049
Received 16 June 2017; Received in revised form 12 August 2017; Accepted 18 August 2017
Available online 19 August 2017

curve to 220 GPa. On the other hand, using the semi-empirical Lindemann melting rule, Mukherjee at al [27] provide the melting curve of Bi up to the same pressure, but the estimated melting temperature is lower than that given by Cox.

Overall, previous studies yield an overview of the Bi phase diagram and behavior across a range of conditions. However, the quantity of precise data for liquid bismuth, in particular, is surprisingly small. Most studies of liquid Bi to date have been restricted to either high temperature at ambient pressure [28–30] or, conversely, to high pressure but ambient temperature [17,18,20]. In fact, the only reference for static determinations of parameters of liquid Bi at simultaneous high temperature and high pressure is Spetzler1l et al. [31] in 1975, and this study was limited to pressures below 1 GPa. We note that Umnov et al. [32] observed anomalies in the electrical conductivity and volume compression of liquid Bi that were attributed to liquid-liquid phase transitions, but this report has not been confirmed.

In 1967, Davis and Gordon [33] introduced the analysis of the EOS based on classical thermodynamic relationships, allowing accurate determination of volume of a liquid as a function of pressure and temperature from experimental adiabatic sound velocity. The method is independent of any knowledge about compression in solid phases. This EOS analysis has been widely used on various materials. Recently, its validity in liquid metals was proved by Ayrinhac [34,35], who showed that the sound velocity as a function of density follows a scaling law valid across the entire metallic state regime.

In this paper, we report ultrasonic measurements of sound velocity of liquid bismuth conducted in a multi-anvil apparatus (MAA) at conditions up to 4.3 GPa and 973 K. Using the experimental data and the sound velocity analysis method, we deduce the EOS of liquid bismuth in the measured pressure range and make comparisons with previous work. Next, given that the solid-solid phase transition boundaries are well-known, we present a means to derive the thermal EOS of the solid phases based on their phase boundaries. Finally, we utilized the EOS of both liquid and solids to calculate the melting curve of bismuth up to 8 GPa based on equality of the thermodynamic potential. We find rather good agreement between the calculated result and available data in the literature, confirming the internal consistency of the method and parameters.

2. Experimental method

The experiments were performed on a MAA (YL-800 t Guilin Guiyue Heavy Industries Co. Ltd., China) at the China Academy of Engineering Physics [36], which has the capability to generate hydrostatic pressure up to approximately 6 GPa. The details of the sample assembly, given in Fig. 1, were described along with the data recording method by Song [37] and Xu [36].

The sample we used in this work is a block of bismuth with 99.99% purity (Alfa). The metal block was cut into small pieces (~ 8.5*3.5*2 mm) using diamond wire cutting, then ground to the size that fits the cavity (3 mm in width, 1.5 mm in depth) in the tungsten carbide sample holder (8 mm in diameter, 6 mm in length). The cavity reminds rigid and keeps the liquid sample thickness effectively constant [36], but NaCl pressure medium is able to push on the lateral ends of the Bi liquid and transmit a hydrostatic pressure to it. The Alumina buffer (8 mm in diameter, 12 mm in length) and Sodium chloride tube (8 mm in inner diameter, 10 mm in outer diameter and 18 mm in length) prevent the sample from leaking.

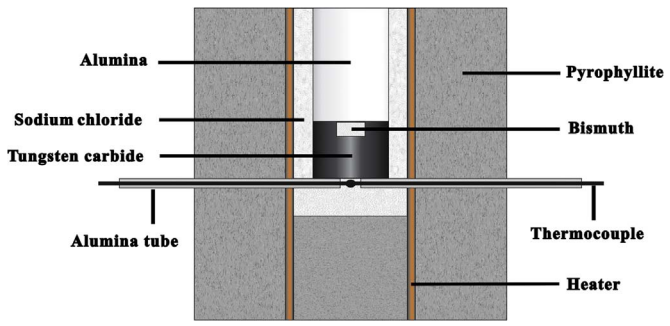

Fig. 1. Schematic diagram of the pressure assembly in the multi-anvil apparatus.

The other parts of the pulse-echo technique measurement system included a longitudinal wave ultrasonic transducer with 10 MHz center frequency and a digital oscilloscope (Wave Runner HRO 66Zi, 12-bit, Teledyne Lecroy, USA), which were used for acoustic signal generation and recording, respectively. When the ultrasonic wave travels along the axis, it will be reflected at each interface, so the reflected signals at the upper and lower interface of the sample could be recorded by the digital oscilloscope. The time delay between the two echoes, Δt, is twice the travel time of the acoustic wave in the sample. The uncertainty in the travel time measurement is less than 1%. As the sample is confined between rigid and nearly incompressible tungsten carbide and alumina parts, the sample thickness Δx remains effectively constant, and the velocity of sound in liquid bismuth is given by $v = (2 \times \Delta x)/\Delta t$.

As with all multi-anvil type pressure devices, the calibration of sample pressure as a function of hydraulic oil pressure and of the offset between the thermocouple reading and the sample temperature in our apparatus are critical steps. For that purpose, we measured the adiabatic sound velocities of liquid bismuth during slow heating at constant hydraulic oil pressures up to 510 kg/cm^2 in 40 kg/cm^2 intervals. In order to calibrate the temperature and the pressure, following the method proposed by Z. Wang [11], we located the melting temperature at each oil pressures by locating a discontinuity in sound velocity of bismuth upon heating. Furthermore, at a hydraulic load of 510 kg/cm^2, we observed two transitions: the solid-solid transition from phase IV to V at thermocouple reading 530 K and then melting from phase V to liquid at 612 K. These two observations provide the information needed to calibration the thermocouple offset. The temperature difference between the two measured transitions was 82 K. According to the phase diagram of bismuth given by Chen [16], at 4.26 GPa the IV-V and V-liquid transition temperatures are 525 K and 608 K, respectively, and the temperature interval between them is 82 K. In a steady-state temperature field the thermal gradient between any two points should be approximately proportional to the temperature; hence, we assume that the difference between the actual temperature of the sample (T) and the temperature reading at the thermocouple (T_{thermo}) should increase linearly with temperature [11]. Thus, the relationship between T and T_{thermo} is estimated as $T(K) = 1.012 \times T_{thermo}(K) - 11.463$ with a maximum misfit of 1 K. Next, given the corrected melting temperature data and the phase diagram from Chen [16], we examined the relationship between the hydraulic oil pressure (P_{oil} in kg/cm^2) and the actual pressure of the sample (P in GPa) based on the nine observations shown in Table 1. The fitted regression equation is $P = -2.45 \times 10^{-6} \times P_{oil}^2 + 0.0101 \times P_{oil} - 0.15$ with a

Table 1
Data used to define thermocouple offset and pressure calibration: melting temperature of Bi from sound-speed discontinuity, measured by thermocouple at various hydraulic oil pressure loads, and the corrected temperature and pressure estimates.

P_{oil} kg/cm^2	T_{thermo} K	T K	P GPa
130	496	490	1.12
150	488	482	1.31
270	486	480	2.40
310	506	500	2.75
350	531	525	3.08
390	541	536	3.42
430	572	567	3.74
470	604	599	4.06
510	627	623	4.36

Table 2
Experimental adiabatic sound velocities of liquid bismuth.

568 K			669 K			770 K			872 K			973 K		
P GPa	v km/s	±	P GPa	v km/s	±	P GPa	v km/s	±	P GPa	v km/s	±	P GPa	v km/s	±
1.12	1.891	0.004	1.12	1.882	0.008	1.12	1.873	0.012	1.12	1.859	0.016	1.12	1.835	0.021
1.31	1.930	0.004	1.31	1.921	0.008	1.31	1.914	0.012	1.31	1.902	0.016	1.31	1.883	0.021
1.50	1.962	0.004	1.50	1.956	0.007	1.50	1.949	0.012	1.50	1.937	0.016	1.50	1.923	0.022
1.68	1.979	0.004	1.68	1.976	0.007	1.68	1.974	0.011	1.68	1.964	0.016	1.68	1.942	0.022
1.86	2.026	0.003	1.86	2.021	0.007	1.86	2.017	0.011	1.86	2.007	0.016	1.86	1.995	0.022
2.04	2.039	0.003	2.04	2.039	0.007	2.04	2.043	0.011	2.04	2.035	0.016	2.04	2.027	0.022
2.22	2.071	0.003	2.22	2.066	0.007	2.22	2.063	0.011	2.22	2.054	0.016	2.22	2.043	0.022
2.40	2.097	0.003	2.40	2.088	0.006	2.40	2.083	0.011	2.40	2.078	0.016	2.40	2.065	0.022
2.57	2.124	0.002	2.57	2.120	0.006	2.57	2.118	0.011	2.57	2.109	0.016	2.57	2.099	0.022
2.75	2.132	0.002	2.75	2.125	0.006	2.75	2.126	0.010	2.75	2.112	0.016	2.75	2.114	0.022
2.92	2.160	0.002	2.92	2.155	0.006	2.92	2.153	0.010	2.92	2.145	0.016	2.92	2.135	0.021
3.08	2.175	0.001	3.08	2.170	0.005	3.08	2.175	0.010	3.08	2.165	0.015	3.08	2.158	0.021
3.25	2.192	0.001	3.25	2.186	0.005	3.25	2.184	0.010	3.25	2.175	0.015	3.25	2.167	0.021
3.42	2.211	0.001	3.42	2.219	0.005	3.42	2.214	0.010	3.42	2.200	0.015	3.42	2.193	0.021
3.58	2.229	0.001	3.58	2.233	0.005	3.58	2.212	0.009	3.58	2.201	0.015	3.58	2.192	0.021
			3.74	2.238	0.004	3.74	2.229	0.009	3.74	2.212	0.014	3.74	2.210	0.021
			3.90	2.243	0.004	3.90	2.241	0.009	3.90	2.229	0.014	3.90	2.220	0.020
			4.06	2.251	0.004	4.06	2.244	0.008	4.06	2.239	0.014	4.06	2.231	0.020
			4.21	2.262	0.003	4.21	2.256	0.008	4.21	2.250	0.014	4.21	2.239	0.020
			4.36	2.273	0.003	4.36	2.269	0.008						

maximum misfit of 0.1 GPa. For the uncertainty of sound velocity, we have to consider the length change in tungsten carbide groove. According to the thermal expansion and bulk modulus of tungsten carbide [38], in our experimental pressure and temperature range, the length change is less than 1.15%.

3. Results and discussion

3.1. EOS and parameters of liquid Bi under HTHP

The adiabatic sound velocities of liquid bismuth as a function of pressure along five different isotherms are presented in Table 2 and Fig. 2. The values of temperature have been corrected using our thermocouple offset calibration and the pressures are based on the calibration polynomial derived above. Literature data for sound velocity of liquid bismuth up to 1 GPa pressure, from Spetzler [31], are also shown in Fig. 2.

The experimental sound velocity data (93 observations, Table 2) determined in this study were fitted to a polynomial function along with zero pressure values from Greenberg [30] (temperature range 544–1000 K):

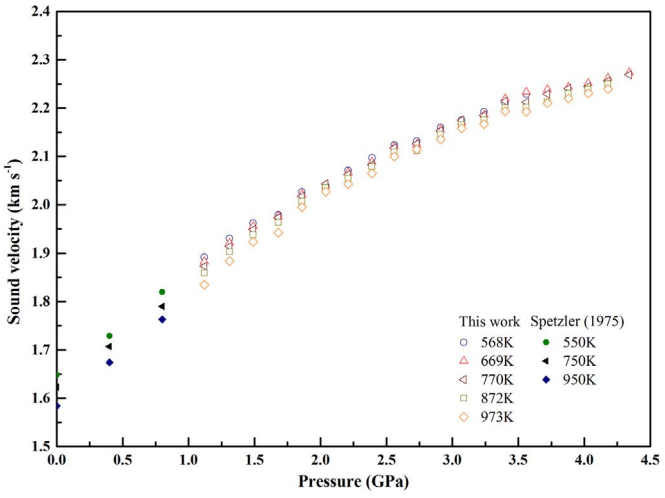

Fig. 2. Adiabatic sound velocity of liquid bismuth along isotherms vs. pressure.

$$v(P, T) = \sum_{i,j} a_{ij}(T-273)^i P^j. \quad (1)$$

The coefficients are shown in Table 3. The regression gives $R^2 > 0.999$ and the maximum difference between the original data in Table 2 and the fitted data using Eq. (1) is less than 0.018 km/s with a reduced $\chi^2 = 5.96$, which is similar to the experimental uncertainties in the original sound velocity data (Table 2). The five coefficients retained in the fit are the only ones found to be significantly different from zero.

To extract the density of liquid bismuth as a function of temperature and pressure from our experimental sound velocity data, we follow the procedure of Ayrinhac [34,35]. The sound velocity v is related to density ρ through the thermodynamic relationships:

$$\alpha = -\frac{1}{\rho}\left(\frac{\partial \rho}{\partial T}\right)_P \quad (2)$$

$$\left(\frac{\partial \rho}{\partial P}\right)_T = \frac{1}{v^2} + \frac{T\alpha^2}{C_P} \quad (3)$$

$$\left(\frac{\partial C_P}{\partial P}\right)_T = -\frac{T}{\rho}\left[\alpha^2 + \left(\frac{\partial \alpha}{\partial T}\right)_P\right], \quad (4)$$

where ρ is the density, v is the sound velocity, α is the isobaric thermal expansion, and C_P is the isobaric heat capacity per unit mass. To start, we fit density data at zero pressure between 544 K and 1000 K given by Stankus [29] to get the expression of density as a function of temperature at zero pressure $\rho(P_0,T)$ and hence the thermal expansion at zero pressure using Eq. (2). The values of $C_P(P_0,T)$ from Gronvold [28] are fitted to a third order polynomial $C_P = 15.049 + 8.191\times10^{-2}T - 1.393\times10^{-4}T^2 + 7.212\times10^{-8}T^3$ with T in K and C_P in $Jmol^{-1}K^{-1}$. Then we can derive the approximate density at an arbitrary reference pressure using Eq. (3) and the resulting density is used to update the value of α_P and C_P at the same pressure with Eqs. (2) and (4). Iteration of this loop leads to converged values of ρ, α_P and C_P at high pressure conditions.

Furthermore, the adiabatic bulk modulus K_S and isothermal bulk modulus K_T can be derived as well, using:

$$K_S = \rho v^2 \quad (5)$$

$$K_T = \frac{K_S}{(1+\alpha\gamma T)}, \quad (6)$$

Table 3
a_{ij} coefficients for $v(P, T) = \sum_{i,j} a_{ij}(T - 273)^i P^j$ with v in km/s, T in K and P in GPa.

i/j	0	1	2
0	1.668 ± 0.021	0.247 ± 0.006	(– 2.431 ± 0.090) × 10^{-2}
1	–	(1.442 ± 0.809) × 10^{-5}	–
2	(– 1.157 ± 0.759) × 10^{-7}	–	–

Table 4
b_{ij} coefficients for $V(P, T) = \sum_{i,j} b_{ij}(T - 273)^i P^j$ with V in m^3 mol^{-1}, T in K and P in GPa.

i/j	0	1	2
0	(2.016 ± 0.001) × 10^{-5}	(–7.021 ± 0.023) × 10^{-7}	(6.336 ± 0.035) × 10^{-8}
1	(2.266 ± 0.042) × 10^{-9}	(–2.643 ± 0.034) × 10^{-10}	–
2	(9.035 ± 4.148) × 10^{-14}	–	–

where γ is the Grüneisen parameter

$$\gamma = \frac{\alpha K_S}{\rho C_P} = \frac{\alpha v^2}{C_P}. \quad (7)$$

Once the relationship between density, temperature and pressure is obtained, an equation for the molar volume (simply the reciprocal of density times the atomic weight) can be fitted to a polynomial form

$$V(P, T) = \sum_{i,j} b_{ij}(T-273)^i P^j, \quad (8)$$

with $R^2 > 0.999$. The coefficients of this fit are listed in Table 4; again the six parameters shown are the only ones significantly different from zero. A tabulated set of all the liquid thermodynamic parameters obtained is given in Table 5.

To test the validity of the polynomial EOS of liquid bismuth, Eq. (8), we also fit our results to the third-order Birch-Murnaghan equation of state (3BM-EOS):

$$P = \frac{3}{2}K_{0,T}(R^{7/3} - R^{5/3})\left[1+\frac{3}{4}(K_0'-4)(R^{2/3}-1)\right], \quad (9)$$

where $R = V_{0,T}/V_{P,T}$, with $V_{0,T}$ is the volume at temperature T and zero pressure and $V_{P,T}$ is the volume at temperature T and pressure P. $K_{0,T}$ is the isothermal bulk modulus and K_0' its pressure derivative, both evaluated at zero pressure. The 3BM-EOS is derived from the finite strain theory of solids, but it has proven to be a reliable and appropriate form for interpolating the volume of liquid metals at high pressure as well [7].

According to Angel [39], $K_{0,T}$ can be approximated as a linear function of temperature up to 1000 K. Coupling the experimental and calculated results above, $K_{0,T}$ can be approximated by:

$$K_{0,T} = -1.3005\times10^{-2}T+31.0930, \quad (10)$$

with a maximum difference of 0.3 GPa at 1000 K. Then, with Eqs. (5)–(7), the pressure derivative of K_T can be written:

$$K_0' = \left(\frac{\partial K_T}{\partial P}\right)_T = 2\rho_0 v_{0,T}\left(\frac{\partial v}{\partial P}\right)_T + \frac{K_{0,S}}{K_{0,T}}, \quad (11)$$

where $v_{0,T}$ is the sound velocity as a function of temperature at ambient pressure and $K_{0,S}$ is the adiabatic bulk modulus at ambient pressure.

In Fig. 3, Spetzler's nine data points [31] were transformed to calculate density at fit to a model of the same form as Eq. (8) using the method described above. Up to 1 GPa, the agreement with the fit to our data using Eq. (8) is exceptionally good, which confirms the accuracy of our data and the consistency with Spetzler [31]. The agreement between Eq. (8) and the fitted 3rd-order Birch-Murnaghan EOS is also reasonably good, with differences from the Spetzler data less than 0.67%, but the two fitting methods diverge somewhat with increasing pressure and temperature. The polynomial form is preferred for fitting our data above 2 GPa or 770 K.

There is no evidence in our data for anomalous compressibility as reported by Umnov et al. [32]. We suspect that their method of thermobaroanalysis did not yield reliable results in this instance, or that our data do not reach sufficient P and T to see the putative liquid structure transition region.

3.2. Calculation of the melting curve of Bi

3.2.1. The melting curve up to 5 GPa

The melting curve of bismuth up to ~ 5 GPa has been report by various of investigators using both experimental [10,12,13,16,40] and theoretical methods [25,26]. Here, combining the data from this study and previous work, we tried to derive the melting curve using a thermodynamic method and to compare to former results. We note that our pressure calibration assumed the melting curve of Bi in advance, so we treat this as a consistency check rather than a primary or absolute measurement of the melting curve.

The fundamental thermodynamic principles of phase equilibrium show that equality of Gibbs free energy is the essential criterion for locating first-order phase transitions such as melting curves in (P, T) space [41,42], and that from an accurate and differentiable free energy function all the thermodynamic properties of a system can be derived. However, the free energy approach requires precise values of thermodynamic parameters; small errors in the relative free energy of two phases can sometimes translate into large errors in the position of phase boundaries. Conversely, accurate phase boundaries translate into precise constraints for estimating free energy functions. Since most of the accurate data reported on bismuth have been obtained at ambient pressure and high temperature [28–30], it is a useful consistency test to calculate the melting curve of phase I. The equation we employ is [43]

$$\Delta H_{Tf} + \int_{Tf}^{T} \Delta C_P(T)dT - T\left(\Delta S_{Tf} + \int_{Tf}^{T} \frac{\Delta C_P(T)}{T}dT\right) = -\int_1^P \Delta V_T(P)dP, \quad (12)$$

where T_f is the fusion temperature of solid bismuth at 1 bar. ΔH_{T_f} and ΔS_{T_f} are the equilibrium enthalpy and entropy of fusion of Bi at 1 bar. $\Delta C_P(T)$ is the specific heat of the liquid minus that of the solid at 1 bar and elevated temperature. $\Delta V_T(P)$ is the specific volume of the liquid minus that of the solid, evaluated iteratively along the fusion curve. It is reasonable to use this equation over the pressure range where phase I and liquid are both at least metastable and their ambient pressure heat capacities can be extrapolated beyond their stability fields.

To calculate the volume of phase I along its melting curve, we employ the Murnaghan EOS [44]:

$$V(P, T) = V(0,T)\left[1+P\left(\frac{K_0'}{K_{0,T}}\right)\right]^{-1/K_0'}. \quad (13)$$

Table 5
Various thermodynamic properties of liquid bismuth up to 973 K, 4.3 GPa.

T K	P GPa	ρ kg/m^3	α × 10^{-5} K^{-1}	γ	K_S GPa	K_T GPa
573	0.0	10,015.77	1.185	2.263	27.27	23.64
573	0.5	10,215.08	1.074	2.336	31.55	27.59
573	1.0	10,390.22	0.992	2.438	36.13	31.73
573	1.5	10,546.01	0.930	2.535	40.62	35.79
573	2.0	10,688.37	0.882	2.590	44.31	39.18
573	2.5	10,820.10	0.838	2.657	48.36	42.89
573	3.0	10,943.25	0.797	2.661	51.44	45.87
573	3.5	11,059.82	0.763	2.679	54.63	48.90
623	0.0	9956.41	1.192	2.284	26.87	22.97
623	0.5	10,160.03	1.078	2.359	31.16	26.90
623	1.0	10,338.43	0.994	2.461	35.77	31.04
623	1.5	10,496.77	0.930	2.561	40.31	35.11
623	2.0	10,641.06	0.880	2.620	44.09	38.55
623	2.5	10,774.54	0.837	2.682	48.03	42.14
623	3.0	10,899.34	0.797	2.689	51.12	45.10
623	3.5	11,017.21	0.762	2.719	54.55	48.32
623	4.0	11,129.41	0.726	2.661	56.60	50.52
673	0.0	9897.06	1.199	2.307	26.46	22.31
673	0.5	10,105.15	1.082	2.383	30.78	26.23
673	1.0	10,286.94	0.995	2.487	35.41	30.35
673	1.5	10,447.91	0.929	2.590	40.01	34.43
673	2.0	10,594.19	0.879	2.653	43.88	37.93
673	2.5	10,729.45	0.836	2.710	47.70	41.40
673	3.0	10,855.91	0.796	2.720	50.81	44.35
673	3.5	10,975.14	0.761	2.760	54.44	47.70
673	4.0	11,088.65	0.725	2.684	56.09	49.60
673	4.3	11,155.09	0.705	2.659	57.48	51.05
723	0.0	9837.70	1.207	2.324	26.02	21.63
723	0.5	10,050.63	1.085	2.404	30.37	25.55
723	1.0	10,235.96	0.996	2.510	35.04	29.68
723	1.5	10,399.55	0.929	2.615	39.68	33.75
723	2.0	10,547.79	0.877	2.688	43.73	37.36
723	2.5	10,684.68	0.834	2.739	47.44	40.71
723	3.0	10,812.60	0.795	2.758	50.66	43.73
723	3.5	10,933.19	0.760	2.776	53.87	46.74
723	4.0	11,048.33	0.725	2.713	55.74	48.81
723	4.3	11,115.61	0.705	2.691	57.17	50.27
773	0.0	9778.35	1.214	2.335	25.58	20.98
773	0.5	9996.17	1.089	2.417	29.96	24.90
773	1.0	10,185.06	0.997	2.526	34.68	29.03
773	1.5	10,351.29	0.929	2.633	39.36	33.10
773	2.0	10,501.48	0.876	2.715	43.57	36.81
773	2.5	10,639.99	0.833	2.761	47.17	40.05
773	3.0	10,769.38	0.794	2.786	50.48	43.11
773	3.5	10,891.32	0.759	2.784	53.31	45.82
773	4.0	11,008.09	0.724	2.733	55.39	48.04
773	4.3	11,076.19	0.705	2.716	56.84	49.51
823	0.0	9719.00	1.221	2.330	25.10	20.34
823	0.5	9941.97	1.093	2.414	29.50	24.24
823	1.0	10,134.68	0.999	2.523	34.24	28.36
823	1.5	10,303.78	0.928	2.631	38.94	32.43
823	2.0	10,456.23	0.874	2.715	43.21	36.15
823	2.5	10,596.58	0.831	2.762	46.81	39.37
823	3.0	10,727.80	0.793	2.788	50.08	42.37
823	3.5	10,851.44	0.758	2.781	52.83	45.02
823	4.0	10,969.88	0.723	2.739	55.05	47.33
823	4.3	11,038.77	0.705	2.716	56.30	48.64
873	0.0	9659.65	1.229	2.309	24.63	19.74
873	0.5	9887.61	1.097	2.395	29.04	23.62
873	1.0	10,083.98	1.000	2.503	33.80	27.74
873	1.5	10,255.78	0.928	2.612	38.53	31.80
873	2.0	10,410.33	0.873	2.697	42.84	35.54
873	2.5	10,552.37	0.830	2.745	46.45	38.74
873	3.0	10,685.27	0.792	2.771	49.68	41.69
873	3.5	10,810.49	0.756	2.760	52.35	44.28
873	4.0	10,930.47	0.723	2.727	54.69	46.67
873	4.3	11,000.11	0.705	2.697	55.76	47.82
923	0.0	9600.30	1.236	2.265	24.12	19.17
923	0.5	9833.42	1.101	2.346	28.49	23.00
923	1.0	10,033.83	1.001	2.449	33.19	27.07
923	1.5	10,208.63	0.928	2.566	38.07	31.21
923	2.0	10,365.40	0.871	2.654	42.47	35.00
923	2.5	10,509.07	0.829	2.699	46.01	38.14
923	3.0	10,643.23	0.791	2.730	49.29	41.10
923	3.5	10,769.68	0.755	2.718	51.96	43.68
923	4.0	10,890.77	0.722	2.688	54.30	46.05
923	4.3	10,961.13	0.705	2.659	55.30	47.14
973	0.0	9540.96	1.244	2.198	23.62	18.66
973	0.5	9778.79	1.106	2.275	27.94	22.44
973	1.0	9982.87	1.002	2.371	32.60	26.47
973	1.5	10,160.33	0.927	2.495	37.61	30.70
973	2.0	10,319.00	0.870	2.585	42.10	34.54
973	2.5	10,464.02	0.827	2.627	45.58	37.62
973	3.0	10,599.16	0.790	2.662	48.90	40.59
973	3.5	10,726.61	0.754	2.650	51.56	43.16
973	4.0	10,848.58	0.721	2.623	53.89	45.51
973	4.3	10,919.54	0.705	2.594	54.82	46.54

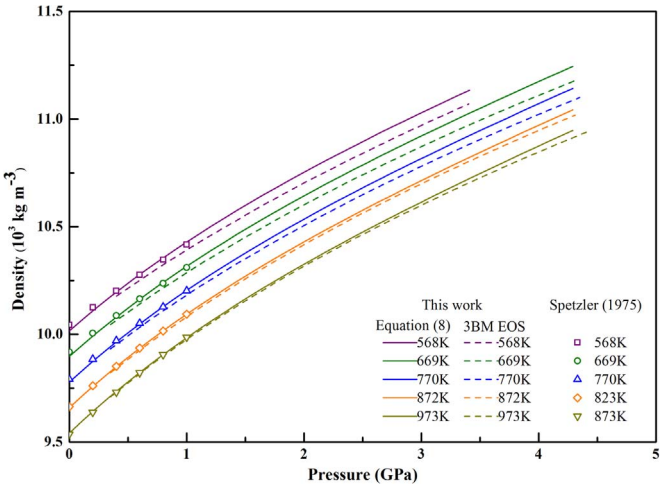

Fig. 3. Fitted isothermal curves for density of liquid bismuth vs. pressure, from the polynomial and Birch-Murnaghan expressions, compared to points representing a similar fit to the data of Spetzler [31].

Stankus [29] and Gronvold [28] reported H, S, C_P and V of both liquid and solid bismuth as a function of temperature at ambient pressure. Moreover, Degtyareva [18] and Li [45] provide values of K_{T0} and K_0' (referenced to zero pressure) for each solid phase. Thus, with Eq. (8) representing the fit to density of liquid Bi based on our new sound speed data, the literature data on solid phase I and ambient P properties of liquid Bi, and Eqs. (12) and (13), we can derive the melting curve of phase I.

To continue calculating the melting curve beyond the first triple point, the parameters of the other solid phases are needed. Only a few of experiments have been performed on these phases, so we have to build the EOS of each solid phase. Therefore, we introduce an approach to obtain the thermal EOS of each subsequent phase at high pressure by making use of the known solid-solid phase boundaries and the Clausius-Clapeyron relation [46]:

$$\frac{dP}{dT} = \frac{\Delta S}{\Delta V}, \tag{14}$$

where dP/dT is the slope at a point along a coexistence curve and ΔV and ΔS are respectively the specific volume change and entropy change of the phase transition at that point. Although this equation only yields the ratio of entropy change to volume change between two coexisting phases when the phase transition boundary is known, it provides in many cases the necessary extra constraint to sequentially construct an EOS for each high-pressure phase.

Previous data on the melting curve of bismuth are mainly grouped into two categories: studies that focus on the lower pressure range (~

Table 6
Data and parameters used in the calculation of each solid phase, with references.

Phase	P GPa	T K	$V_{P,T}$ m^3/mol	Ref.	$K_{0,T}$ GPa	K_0'	Ref.	Phase boundary	Ref.
II	1.73	456	1.954×10^{-5}	[26]	44.5	4.7	[45]	I-II	[16]
	2.7	298	1.888×10^{-5}	[18]					
III	1.7	456	1.844×10^{-5}	[26]	55	4	[18]	II-III	[16]
	3.6	298	1.784×10^{-5}	[18]					
V	5.26	447	1.732×10^{-5}	[26]	56	4.5	[18]	III-V	[16]
	8.5	298	1.651×10^{-5}	[18]					
IV	1.7	456	1.844×10^{-5}	[26]	55	4.8	[45]	V-IV	[16]
	3.9	503	1.813×10^{-5}	[16]					

5 GPa) where several phase transitions occur, and those that focus on higher pressures along the phase V melting curve. First, we will try to calculate the melting curve up to ~ 5 GPa for comparison to studies in the first category.

Considering that the melting curves in this pressure range are restricted to a temperature range of only a few hundred K, it should be an adequate approximation to treat the zero-pressure volume of each solid phase as linear in temperature. For phase II, for example, we assume

$$V^{II}(0,T) = m_1 T + m_2 \tag{15}$$

where m_1 and m_2 are constants, T is the temperature in K, and V is the molar volume in $m^3 mol^{-1}$. With the two P-V-T data and the K_{T0} and K_0' given in the first row of Table 6, Eqs. (13) and (15) lead to two linear equations with unknowns m_1 and m_2, which are easily solved. The results are listed in Table 7.

Next, given the phase boundary I-II from the internally consistent phase diagram of Chen [16], which synthesizes a number of previous studies [10,14,15], we can estimate the value of dP/dT along the phase boundary curve. Using the data from references [18,28,29], and [44]; Eqs. (13) and (15); and a Maxwell relation between thermal expansion and the pressure derivative of entropy, we have everything we need to estimate $V^I_{P,T}$, $S^I_{P,T}$ and $V^{II}_{P,T}$ at any (P,T) point along the phase boundary, so the only unknown in a re-arranged Clausius-Clapeyron equation is the entropy of phase II:

$$S^{II}(P,T) = \frac{dP}{dT}(V^{II}(P,T) - V^{I}(P,T)) + S^{I}(P,T). \tag{16}$$

The resulting estimates of entropy at high pressure are brought back down to ambient pressure, again using the Maxwell relation, to obtain a series of values of entropy of phase II at zero pressure and various temperatures

$$S(0,T) = S(P,T) - \int_0^P -\left(\frac{\partial V}{\partial T}\right)_P dP, \tag{17}$$

which can be fit to a polynomial. We find that the entropy of phase II as a function of temperature at zero pressure is adequately represented with three terms

Table 7
Fit coefficients of Eqs. (15) and (18).

Coefficients					
phase	T-V_0		T-S_0		
	m_1	m_2	n_1	n_2	n_3
Solid-II	2.1208×10^{-9}	1.9283×10^{-5}	-6.5325×10^{-5}	0.1172	−23.2778
Solid-III	3.8101×10^{-10}	1.8831×10^{-5}	-5.2076×10^{-5}	0.1031	−15.1952
Solid-IV	6.2064×10^{-9}	1.6149×10^{-5}	-11.9416×10^{-5}	0.0949	2.7681
Solid-V	1.3195×10^{-9}	1.8142×10^{-5}	-4.8251×10^{-5}	0.0906	−8.1731

$$S^{II}(0,T) = n_1 T^2 + n_2 T + n_3, \tag{18}$$

where n_1, n_2, n_3 are constants; T is temperature in K; and S is the entropy in $J\,mol^{-1}K^{-1}$. Sequential application of the same method using data on the other phase boundaries and the values of $K_{0,T}$ and K_0' for phases I, II, III and IV from Li [45] and Degtyareva [18] leads in turn to fit parameters for $V_{0,T}$ and $S_{0,T}$ for each solid phase in the order of I-II-III-V-IV, see Table 7.

Once we have obtained thermodynamic parameters for each phase, we return to Eq. (14) to estimate the initial slope dP/dT of the (metastable) melting curve of each phase at ambient pressure [16] from our equations for $V^I_{0,T}$, $S^I_{0,T}$, $V^{Liq}_{P,T}$ and $S^{Liq}_{0,T}$. The resulting slope is used to obtain the next melting point at a small increment of pressure. Using the ambient pressure stable melting point of phase I as an initial condition for integration, this method allows us to construct the melting curve of phase I up to its intersection with the extension of the I-II phase transition boundary. At this point we replace $V^I_{0,T}$, $S^I_{0,T}$ with $V^{II}_{0,T}$, $S^{II}_{0,T}$ and continue the integration to derive the melting curve of phase II. Making use of the volume and entropy equations of each solid phase and the solid-solid phase boundaries that intersect the liquidus in turn, we construct the complete melting curve of bismuth up to 5 GPa.

The calculated equilibrium boundary between solid phase and liquid bismuth is shown in Figs. 4 and 5. In Fig. 4, results using both Gibbs and Clausius-Clapeyron equations are presented, together with direct experimental constraints. Both of our calculation results agree well with the data from the static work [10,12,13] and the deviation in temperature is less than 5 K compared with the work done by Klement [10]. At the I-II-liquid triple point pressure (1.67 GPa), the temperature difference between these two calculation results is ~ 4.2 K. This agreement not only establishes the accuracy of the liquid volume deduced from Eq. (8), but also demonstrates the feasibility of our calculation process. It is worth noting that the experiments of Bundy [40], which were performed under non-hydrostatic pressure conditions, suggest a concave-upwards phase boundary between solid I and liquid. On the other hand, the thermodynamic calculation and static data from hydrostatic experiments agree on a convex-upwards melting curve, suggesting that hydrostatic pressure experiments are more reliable. Fig. 5 presents a comparison of our work with previous experimental data and theoretical calculation results [26]. Overall, the melting curves are fully consistent in the stability fields of phases I and II, up to 2.5 GPa, with the differences among estimated melting temperatures no larger than 8 K. Discrepancies in the placement of the liquid-II-IV triple point then lead to a separation in melting temperatures of up to 23 K from 2.5 to 4 GPa. The accumulation of difference in estimated properties leads to even larger differences above 4 GPa. Our

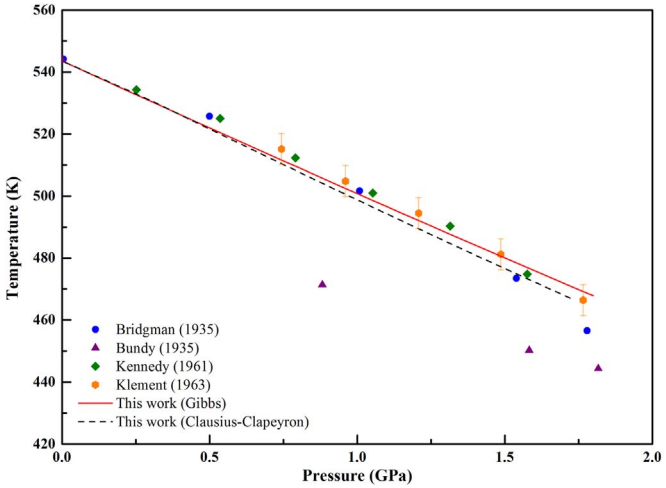

Fig. 4. The transition boundary between phase I and liquid phase.

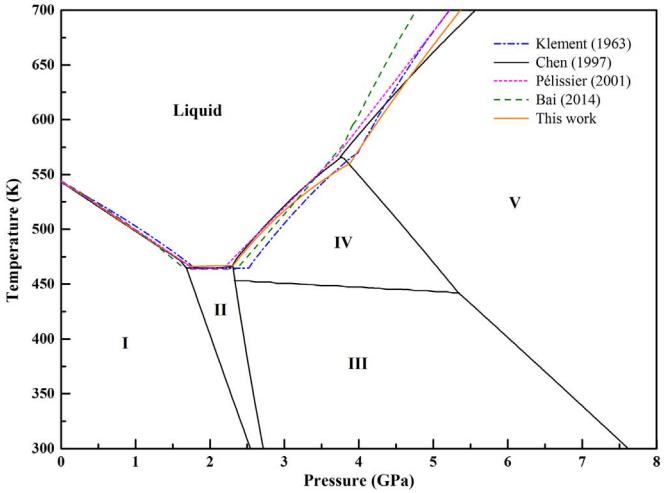

Fig. 5. The melting curve of bismuth calculated using the Clausius-Clapeyron equation. Solid-solid phase transition boundaries follow those adopted by Chen [16].

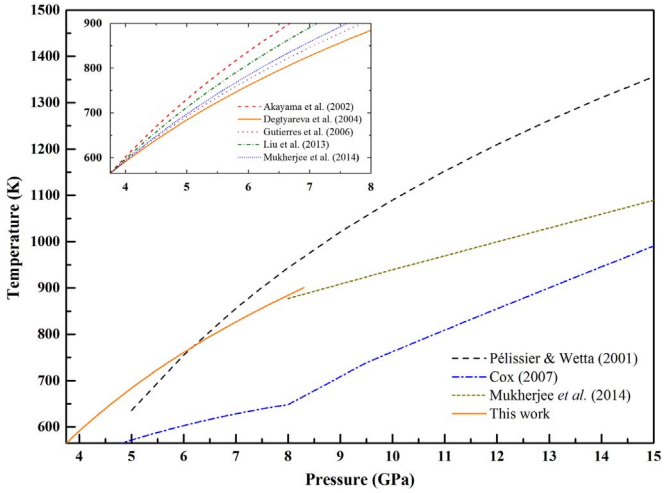

Fig. 6. Calculated melting curve of Phase V (bcc) Bi in the high-pressure range, alongside previous theoretical estimates. The inset shows the results using each $K_{0,T}$ and K_0' pair from Table 8.

calculated result is most similar overall to the melting curve of Pélissier [47], from which the largest difference in temperature is 22 K at 3.9 GPa. Because the calculation order we followed is I-II-III-V-IV, uncertainty in the phase diagram leads to the largest deviations in the slope of the melting curve of phase IV.

3.2.2. The melting curve beyond 5 GPa

Published estimates of the melting curve of Bi at higher pressures and temperatures have mainly been derived from theoretical considerations. Based on a self-consistent Einstein approximation, Pélissier & Wetta [47,48] first calculated the melting curve of bcc bismuth (phase V) up to 60 GPa, an estimate frequently cited by later papers [22,23,47,49]. Then in 2007, Cox [25] provided an empirical model which made modifications to a previous study by Johnson et al. [24] and gave the EOS of each phase of bismuth including liquid, as well as the melting curve up to 50 GPa. Recently, Mukherjee [27] used first-principles calculations and a Lindemann melting rule to estimate a melting temperature of 902 K at pressure ~ 8 GPa.

Experimental data on high-pressure melting of Bi are limited to shock experiments along the principal Hugoniot and releases from such Hugoniot states, which only constrain the melting curve in a narrow pressure range. A sharp increase in short-wavelength optical emissivity from a shocked Bi-LiF interface and a region of low P-T slope along the Hugoniot were interpreted to reveal onset of partial melting along the Hugoniot at about 30 GPa and 2300 K, followed by complete melting at 45 GPa and ~ 2600 K [21]. On the other hand, Partouche-Sebban et al. [22] noted that these observations of a Bi-LiF interface do not constrain melting along the Bi Hugoniot but rather in partial release states; they suggested instead that the shock melting temperatures are lower, ~ 1250–1700K, and that melting is achieved at lower pressures, from ~ 18–28 GPa, which is in agreement with the theoretical calculation by Pélissier & Wetta [48].

To compare these results to our method of calculation, first we must verify whether the fits to the ambient-pressure volume and entropy of phase V (bcc bismuth) in Table 7 remain valid up to the higher temperature range required to model melting at higher pressures. For the ambient pressure entropy, unfortunately, the quadratic polynomial fit with negative T^2 coefficient, given in Table 7, leads to a maximum in the entropy of phase V at 939 K, followed by decrease in entropy with increasing temperature beyond that point. This is an unphysical result, contrary to the thermodynamic stability criterion that requires the heat capacity to be strictly positive and entropy to always increase with temperature. By coincidence, perhaps, the entropy of liquid bismuth was calibrated by Gronvold [28] up to a maximum temperature of 940 K. From these two limits, we estimate that we can define the entropy of fusion of phase V well up to ~ 900 K. It is also challenging to estimate the temperature range over which our linear estimate for the ambient pressure volume of bcc bismuth is valid. However, Stankus [29] showed that the ambient pressure volume of liquid bismuth is linear with temperature up to at least 1600 K. Hence, we will conservatively assume that the volume of phase V (bcc bismuth) remains linear with temperature up to at least 900 K. We will therefore limit our calculation of the fusion curve of phase V to the interval from the triple point of phases IV, V and liquid (3.75 GPa, 565 K, from Chen [18]) up to the pressure where the melting curve reaches 900 K. Using the same procedure as described above to integrate the Clausius-Clapeyron equation, the melting curve up to 900 K is shown in Fig. 6 alongside previous theoretical estimates.

In fact, the equation of state of bcc (phase V) bismuth remains somewhat uncertain. Table 8 gives several published pairs of $K_{0,T}$ and K_0' [17,19,20,27] for bcc Bi and the pressure limits up to which each EOS estimate was constrained. In the inset to Fig. 6, we demonstrate the sensitivity of our melting point estimate to the EOS of the solid phase by showing the calculated melting curves using each of these $K_{0,T}$ and K_0' pairs. The effect is significant; the melting curve might cross 900 K at a pressure anywhere from 6.5 to 8 GPa, depending on the EOS of phase V.

As Fig. 6 shows, our preferred melting curve passes through ~ 8 GPa at ~ 900 K, close to the result given by Mukherjee et al. [27]. For this calculation, we adopted the values of $K_{0,T}$ and K_0' from Degtyareva [18], the same as we used in calculating the melting curve up to ~ 5 GPa. This curve, while very similar to that of Mukherjee et al. [27], is notably lower in slope than the estimate from Pélissier & Wetta[44]. A different choice of $K_{0,T}$ and K_0' can yield a slope more comparable to that of Pélissier & Wetta,[44] though offset because their curve does not pass through the triple point from Chen[18] used to anchor our curve. We do not find a plausible set of parameters that yields a melting curve similar to that of Cox[22]. Although our ultrasonic data contribute

Table 8
Zero-pressure bulk modulus and its pressure derivative for bcc bismuth from various estimates.

$K_{0,T}$ GPa	K_0'	Pressure range GPa	Reference
54.7	4.9	~ 222	Akayama et al. [17]
52	4.6	~ 191	Gutiérrez et al. [19]
42.7	5.3	~ 55	Liu et al. [20]
58.9	4.49	~ 220	Mukherjee et al. [27]

significant constraints to our ability to estimate high pressure melting curves, it remains challenging to extrapolate this result very far. The challenge partly lies in the significant contribution of solid compressibility to volumes of fusion at high pressure, and partly in the need to estimate ambient pressure properties at temperatures above the measurable stability range of the phases of interest. Nevertheless, our success up to ~ 900 K and 8 GPa confirms that the thermodynamic method and the analysis of sound speed to define the liquid equation of state are reliable approaches when sufficient data are available.

4. Conclusion

In this work, we demonstrate a thermodynamic method for calculating the melting curve of bismuth using available data and new ultrasonic measurements of the liquid phase. The sound velocity of liquid Bi up to 4.3 GPa and 973 K was determined by the ultrasonic pulse echo technique in a multi-anvil apparatus. The sound velocity data are used to derive the equation of state parameters of liquid bismuth at high pressure and temperature, including density, molar volume, thermal expansion and isothermal bulk modulus. The precision of the data is sufficient to constrain a linear relation between isothermal bulk modulus and temperature, and to estimate the pressure derivative of the isothermal bulk modulus. Armed with this liquid equation of state, we attempt a thermodynamic calculation of the phase diagram of Bi. We make use of well-measured solid-solid phase transition boundaries to construct, in sequence, the thermal EOS of each solid phase. This combination yields an internally consistent melting curve that, up to 5 GPa, accurately reproduces direct measurements from static experiments. In the less certain higher pressure range, we extrapolate our melting curve of the bcc phase V up to 8 GPa for comparison to estimates from shock wave experiments and find reasonable agreement, depending on the adopted equation of state of the bcc phase. This work not only confirms the stringent self-consistency required to match the experimental phase diagram of bismuth, but also proves the feasibility of the thermodynamic method once the sound velocity of the liquid at elevated temperature and pressure is known with sufficient precision.

Acknowledgments

This work was supported by the Strategic Priority Research Program (B) of the Chinese Academy of Sciences (XDB 18010401); the National Key Laboratory of Shock Wave and Detonation Physics, Institute of Fluid Physics, Chinese Academy of Engineering Physics; The West Light Program from Chinese Academy of Sciences; The US National Science Foundation, award EAR-1426526, and Chinese Council Scholarship. The authors are grateful to Professor Wenge Zhou at Institute of Geochemistry, Chinese Academy of Sciences for helpful discussions and Liang Xu at National Key Laboratory of Shock Wave and Detonation Physics, Institute of Fluid Physics, Chinese Academy of Engineering Physics for supervising the experiments.

References

[1] D. Errandonea, Improving the understanding of the melting behaviour of Mo, Ta, and W at extreme pressures, Phys. B: Condens. Matter 357 (2005) 356–364.
[2] Z.L. Liu, X.F. Li, X.L. Zhang, L.C. Cai, F.Q. Jing, Phase transition and thermodynamic properties of Sr under high pressure, Phys. B 406 (2011) 4518–4522.
[3] D. Alfè, G.D. Price, M.J. Gillan, Iron under Earth's core conditions: liquid-state thermodynamics and high-pressure melting curve fromab initiocalculations, Phys. Rev. B 65 (2002).
[4] C. Song, D. Li, Y. Xu, B.C. Pan, C.S. Liu, Z. Wang, Ab initio molecular dynamics study of temperature dependent structure properties of liquid lead–bismuth eutectic alloy, Phys. B: Condens. Matter 429 (2013) 6–11.
[5] S. Arafin, R.N. Singh, A.K. George, Melting of metals under pressure, Phys. B 419 (2013) 40–44.
[6] T. Komabayashi, J. Kato, K. Hirose, S. Tsutsui, S. Imada, Y. Nakajima, A.Q.R. Baron, Temperature dependence of the velocity-density relation for liquid metals under high pressure: implications for the Earth's outer core, Am. Mineral. 100 (2015) 2602–2609.
[7] O.L. Anderson, D.G. Isaak, Calculated melting curves for phases of iron, Am. Mineral. 85 (2000) 376–385.
[8] J.F. Wax, R. Albaki, J.L. Bretonnet, Diffusion coefficient of liquid alkali metals near the melting point, J. Non-Cryst. Solids 312–314 (2002) 187–190.
[9] J.F. Wax, N. Jakse, I. Charpentier, Static structure of liquid alloys of alkali metals, Phys. B: Condens. Matter 337 (2003) 154–164.
[10] W. Klement, A. Jayaraman, G.C. Kennedy, Phase diagrams of arsenic, antimony, and bismuth at pressures up to 70 kbars, Phys. Rev. 131 (1963) 632–637.
[11] Z.G. Wang, Y.G. Liu, Y. Bi, W. Song, H.S. Xie, Hydrostatic pressure and temperature calibration based on phase diagram of bismuth, High. Press. Res. 32 (2012) 167–175.
[12] P.W. Bridgman, Polymorphism, principally of the elements, up to 50,000 kg/cm(2), Phys. Rev. 48 (1935) 893–906.
[13] G.C. Kennedy, R.C. Newton, The effect of pressure on the electromotive force of a platinum-bismuth thermocouple, J. Geophys. Res. 66 (1961) 1491–1493.
[14] J.C. Haygarth, H.D. Luedmann, I.C. Getting, G.C. Kennedy, Determination of portions of the bismuth III–V and IV–V equilibrium boundaries in single-stage piston-cylinder apparatus, J. Phys. Chem. Solids 30 (1969) 1417–1424.
[15] C.W.F.T. Pistorius, Phase relations and structures of solids at high pressures, Progress. Solid State Chem. 11 (1976) 1–151.
[16] J.H. Chen, H. Iwasaki, T. Kikegawa, Structural study of the high-pressure-high-temperature phase of bismuth using high energy synchrotron radiation, J. Phys. Chem. Solids 58 (1997) 247–255.
[17] Y. Akahama, H. Kawamura, A.K. Singh, Equation of state of bismuth to 222 GPa and comparison of gold and platinum pressure scales to 145 GPa, J. Appl. Phys. 92 (2002) 5892–5897.
[18] O. Degtyareva, M.I. McMahon, R.J. Nelmes, High-pressure structural studies of group-15 elements, High Press. Res. 24 (2004) 319–356.
[19] G. Gutiérrez, E. Menéndez-Proupin, A.K. Singh, Elastic properties of the bcc structure of bismuth at high pressure, J. Appl. Phys. 99 (2006) 103504.
[20] L. Liu, H.X. Song, H.Y. Geng, Y. Bi, J.A. Xu, X.D. Li, Y.C. Li, J. Liu, Compressive behaviors of bcc bismuth up to 55 GPa, Phys. Status Solidi B 250 (2013) 1398–1403.
[21] E. Blanco, J.M. Mexmain, P. Chapron, Temperature measurements of shock heated materials using multispectral pyrometry: application to bismuth, Shock Waves 9 (1999) 209–214.
[22] D. Partouche-Sebban, D.B. Holtkamp, J.L. Pélissier, J. Taboury, A. Rouyer, An investigation of shock induced temperature rise and melting of bismuth using high-speed optical pyrometry, Shock Waves 11 (2002) 385–392.
[23] J.L. Pélissier, D. Partouche-Sebban, Pyrometry measurements on shock-heated bismuth using PMMA and sapphire windows, Phys. B: Condens. Matter 364 (2005) 14–28.
[24] J.N. Johnson, D.B. Hayes, J.R. Asay, Equations of state and shock-induced transformations in solid I-solid II-liquid bismuth, J. Phys. Chem. Solids 35 (1974) 501–515.
[25] G.A. Cox, A multi-phase equation of state for bismuth, in: M. Elert, M.D. Furnish, R. Chau, N.C. Holmes, J. Nguyen (Eds.), Shock Compression of Condensed Matter – 2007, Pts 1 and 2, American Institute of Physics, Melville, 2007, pp. 151–154.
[26] J. Bai, J. Yu, T. Wang, Numerical investigation of bismuth unloading solidification with abnormal melting characteristic, World J. Mech. 2014 (2014).
[27] D. Mukherjee, B.D. Sahoo, K.D. Joshi, S.C. Gupta, On equation of state, elastic, and lattice dynamic stability of bcc bismuth under high pressure: ab-initio calculations, J. Appl. Phys. 115 (2014) 7.
[28] F. Grønvold, E. Larsen, J.E. Moreira, O.F. Nielsen, U. Skoglund, Heat capacity and thermodynamic properties of bismuth in the Range 300 to 950 K. Fusion Characteristics, Acta Chem. Scand. 29a (1975) 945–955.
[29] S.V. Stankus, R.A. Khairulin, A.G. Mozgovoi, V.V. Roshchupkin, M.A. Pokrasin, An experimental investigation of the density of bismuth in the condensed state in a wide temperature range, High Temp. 43 (2005) 368–378.
[30] Y. Greenberg, E. Yahel, M. Ganor, R. Hevroni, I. Korover, M.P. Dariel, G. Makov, High precision measurements of the temperature dependence of the sound velocity in selected liquid metals, J. Non-Cryst. Solids 354 (2008) 4094–4100.
[31] H. Spetzler1l, M. Meyer, T. Chan, Sound velocity and equation of state of liquid mercury and bismuth at simultaneous high pressure and temperature, High. Temp.-High. Press. 7 (1975) 481–496.
[32] A.G. Umnov, V.V. Brazhkin, S.V. Popova, R.N. Voloshin, Pressure temperature diagram of liquid bismuth, J. Phys.-Condens. Matter 4 (1992) 1427–1431.
[33] L.A. Davis, R.B. Gordon, Compression of mercury at high pressure, J. Chem. Phys. 46 (1967) 2650–2660.
[34] S. Ayrinhac, M. Gauthier, L.E. Bove, M. Morand, G. Le Marchand, F. Bergame, J. Philippe, F. Decremps, Equation of state of liquid mercury to 520 K and 7 GPa from acoustic velocity measurements, J. Chem. Phys. 140 (2014) 244201.
[35] F. Decremps, M. Gauthier, S. Ayrinhac, L. Bove, L. Belliard, B. Perrin, M. Morand, G. Le Marchand, F. Bergame, J. Philippe, Picosecond acoustics method for measuring the thermodynamical properties of solids and liquids at high pressure and high temperature, Ultrasonics 56 (2015) 129–140.
[36] L. Xu, Y. Bi, X. Li, Y. Wang, X. Cao, L. Cai, Z. Wang, C. Meng, Phase diagram of tin determined by sound velocity measurements on multi-anvil apparatus up to 5 GPa and 800 K, J. Appl. Phys. 115 (2014) 164903.
[37] W. Song, Y. Liu, Z. Wang, C. Gong, J. Guo, W. Zhou, H. Xie, Note: measurement method for sound velocity of melts in large volume press and its application to liquid sodium up to 2.0 GPa, Rev. Sci. Instrum. 82 (2011) 086108.
[38] K.D. Litasov, A. Shatskiy, Y.W. Fei, A. Suzuki, E. Ohtani, K. Funakoshi, Pressure-volume-temperature equation of state of tungsten carbide to 32 GPa and 1673 K, J. Appl. Phys. 108 (2010) 7.

[39] R.J. Angel, Equations of state, Rev. Mineral. Geochem 41 (2000) 35–59.
[40] F.P. Bundy, Phase diagram of bismuth to 130,000 kg/cm 2500° C, Phys. Rev. 110 (1958) 314.
[41] P. Song, L.C. Cai, Multiphase equation of state for lead, Phys. B 405 (2010) 1509–1512.
[42] F. Xi, L.C. Cai, Theoretical study of melting curves on Ta, Mo, and W at high pressures, Phys. B 403 (2008) 2065–2070.
[43] Q. Liu, T.J. Tenner, R.A. Lange, Do carbonate liquids become denser than silicate liquids at pressure? Constraints from the fusion curve of K_2CO_3 to 3.2 GPa, Contrib. Mineral. Petrol. 153 (2007) 55–66.
[44] V. Singh, A.K. Gautam, K.S. Singh, Analysis of a P–V–T relationship for MgO, Phys. B: Condens. Matter 352 (2004) 164–171.
[45] Y.H. Li, J.Z. Chang, X.M. Li, Y.Y. Yu, C.D. Dai, L. Zhang, Multiphase equation of states of solid and liquid phases for bismuth, Acta Phys. Sin. 61 (2012) 046201.
[46] Q.L. Cao, H. Duo-Hui, L. Qiang, F.H. Wang, C. Ling-Cang, Z. Xiu-Lu, J. Fu-Qian, Improving the understanding of the melting curve of tantalum at extreme pressures through the pressure dependence of fusion volume and entropy, Phys. B 407 (2012) 2784–2789.
[47] N. Wetta, J.L. Pélissier, A model-potential approach for bismuth: ii. behaviour under shock loading, Phys. A: Stat. Mech. Appl. 289 (2001) 479–497.
[48] J.L. Pélissier, N. Wetta, A model-potential approach for bismuth (I), Densif. Melt. Curve Calc. Phys. A: Stat. Mech. Appl. 289 (2001) 459–478.
[49] D. Partouche-Sebban, J.L. Pelissier, Emissivity and temperature measurements under shock loading, along the melting curve of bismuth, Shock Waves 13 (2003) 69–81.